



Insulator defect detection in transmission line based on an improved lightweight YOLOv5s algorithm



Liangliang Wei^a, Jun Jin^a, Kaiyuan Deng^a, Han Liu^{b,*}

^a School of Intelligent Systems Engineering, Sun Yat-Sen University, Guangzhou 510275, China

^b Graduate School of Engineering, Kyoto University, Kyoto, 6158540, Japan

ARTICLE INFO

Keywords:

Attention mechanism
Defect detection
Insulator
UAV
YOLOv5s

ABSTRACT

As one of the most important components on the transmission line, the insulator is prone to failure, which affects the safe operation of electrical power system. Hence, it is crucial to accurately detect the insulator defects for further maintenance in time. Recently, with the development of artificial intelligence and target detection algorithms, the insulator defect detection has received more and more attention. However, there are still existing some difficulties: insufficient samples and low detection accuracy. To improve the accuracy of insulator defect detection, this paper proposes an auto-detection method based on an improved lightweight YOLOv5s model. First, this paper introduces the basic network frame of YOLOv5s and proposes an improved algorithm by utilizing the GIoU loss function, Mish activation function, and CBAM module. Then, performs data enhancement in the insulator dataset to enhance the robustness of the model. Finally, trains and tests the improved YOLOv5s model, and compares it with traditional target detection algorithms. Compared with traditional target detection algorithms, the AP value of the proposed algorithm in detecting insulator defects can be improved by 5 %. The results demonstrate the improved algorithm proposed in this paper can effectively identify and position the insulator defects.

1. Introduction

The insulator is one of the most important parts of the transmission line, playing an important role in supporting the conductors, preventing current leakage or short circuits, and thereby safeguarding the safe and stable operation of the power system [1]. To ensure the long-term stable operation of the transmission line, it is imperative to regularly inspect and check the parts for any defects [2,3]. Since the insulator is exposed to the natural environment at all times, the insulator is prone to aging in severe natural environments and complex electromagnetic environments, resulting in the damage and loss of the insulators. Short circuits or trips of transmission lines caused by insulator aging have brought a lot of economic losses [4,5]. The earliest defective insulators are usually detected through manual inspection, with workers visiting the site to

observe the appearance of the insulator and measure its temperature [6]. However, the efficiency and accuracy of this approach are somewhat limited. In recent years, the utilization of Unmanned Aerial Vehicles (UAVs) for transmission line patrols has become increasingly prevalent [7]. During the UAV patrol, it can collect data on transmission lines through sensors mounted on the drone, and perform long distance insulator fault diagnosis [8]. UAVs have shown significant advantages in inspection work due to their efficient and flexible characteristics [9,10]. But with the extension of UAV patrol, new problems have arisen: a large number of image data produced on patrol need a manual inspection and waste lots of time [11]. Therefore, the automatic detection demand for the image of transmission line insulators has arisen, and holds the potential to significantly enhance the efficiency and accuracy of inspection work, ensuring the safe and reliable operation of the power system [12].

Abbreviation list: AP, Average Precision; BPR, Best possible recall; BN, Batch Normalization; CBS, Conv+BN+SiLU; CBAM, Convolutional Block Attention Module; CIoU, Complete Intersection over Union; CSP, Cross Stage Partial; DIoU, Distance Intersection over Union; D-S, Dempster-Shafer evidence theory; ECANet, Efficient Channel Attention Network; EIoU, Efficient Intersection over Union; FP, False Positve; FPS, Frames Per Second; GIoU, Generalized Intersection over Union; HSV, Hue, Saturation, Value; IoU, Intersection over Union; mAP, Mean Average Precision; NMS, Non maximun suppression; P-R, Precision, Recall; RCNN, Region Convolutional Neural Networks; ReLU, Rectified Linear unit; SSD, State space decomposition; SiLU, Sigmoid Linear Union; SPPF, Spatial Pyramid Pooling Fast; SVM, Support Vector Machine; TP, True Positive; UAV, Unmanned Aerial Vehicle; YOLO, You Only Look Once.

* Corresponding author.

E-mail address: liuhan0103@163.com (H. Liu).

Some researchers have proposed traditional image processing techniques to detect the transmission line insulator defect. Liao and An [13] proposed a multiscale and multi-feature method to extract local features, and then position damaged insulators by training local features. Yu et al. [14] proposed an active profile model to segment insulators based on the shape and texture features. Wu and An [15] proposed a semi-local operator under the Beltrami framework to extract the surface nonuniform texture features. However, the images of insulators usually have different natural environmental backgrounds, and the insulators of different materials have different textures and postures. Traditional image processing methods require manual feature design, which limits their adaptability in complex or dynamic environments. Meanwhile, traditional image processing methods are sensitive to noise and interference, resulting in poor robustness. Hence, the above methods make it difficult to classify the insulators of different materials and different levels of damage in images with complex backgrounds.

With the development of artificial intelligence, machine learning methods have been applied to insulator defect detection. Gencoglu and Uyar [16] proposed a least squares support vector machine (SVM) combined with a particle swarm optimization model to estimate the critical flashover voltage on polluted insulators. Murthy et al. [17] developed an SVM combined with wavelet multi-resolution analysis to accomplish the insulator defect detection. Singh et al. [18] proposed a Gaussian Kernel SVM to classify the insulator defect based on various geometrical morphological, intensity, and statistical features. Traditional machine learning methods extract image features through various methods and then input the features into SVM or other regression methods for insulator detection. However, although traditional machine learning methods have good robustness in the performance of insulator detection, but have a poor defect detection effect on UAV aerial images, especially for small targets.

Recently, with the development of deep learning, a series of target detection algorithms have been proposed, consisting of two-stage target detection algorithms and one-stage target detection algorithms [19]. Among the two-stage target detection algorithms, there are RCNN, and Faster RCNN [20], which first extract candidate regions and then detect them. Lei and Sui [21] used the Faster RCNN algorithm to transform the insulator classification problem into the insulator detection and identification problem. Hao et al. [22] used the cross-stage and residual split attention network with a feature pyramid network to solve the small-target insulator defect detection. Dian et al. [23] introduced the transformer architecture into Faster RCNN to focus more on the recommended regions of the insulators and improve the feature extraction efficiency. The two-stage detection algorithm would intercept the image areas of suspected insulators and further classify them. It can improve the detection accuracy to a certain extent, but the detection speed is slow. Moreover, for insulator defects, the image area of the insulator defect will contain more background information rather than insulator-related information, with too few related features, which hurts further classification.

One-stage target detection algorithm includes SSD [24] and YOLO algorithms [25,26,27], which directly determine the class and position of the target through a neural network. Xiao et al. [28] utilized the method of combining the SSD algorithm and fine-tuning strategy to detect insulator defects. Chen et al. [29] utilized the YOLOv3 algorithm to detect power components. The YOLO algorithm achieves a balance between accuracy and speed, and many scholars have adopted the YOLO algorithm for insulator detection. He et al. [30] proposed a Multi-Layer Information Fusion and Attention Mechanism Network based on YOLOv4 for insulator detection. Han et al. [31] introduced an ECANet module to enhance the separation of background and target, and strengthen the detection of small targets. Zhou et al. [32] introduced an attention mechanism that fuses the channels and locations, which enables the model to quickly capture insulator regions.

In addition, some scholars proposed multiple neural networks to cascade and split insulator detection into multiple steps, sacrificing a

certain speed to achieve better detection results. Huang et al. [33] used the YOLOv5s network to locate the insulator area and utilized the DenseNet201 network to further distinguish whether there was a fault in the insulator. Yang et al. [34] proposed an improved YOLOv3 algorithm to locate insulator positions and then combined it with Dempster-Shafer (D-S) evidence theory to detect the insulator defects. However, it is equivalent to splitting the two-stage algorithm and has a certain amount of information waste between the networks.

Therefore, there still exist some challenges to limit the development of insulator defect detection. Firstly, in aerial photography images, due to the distance between the UAV and the electric tower, the proportion of the insulators captured is not significant in the aerial imagery which puts higher requirements on the information utilization by neural networks. Secondly, compared to the insulators, the proportion of insulator defect parts is smaller, so the error in an IoU calculation will significantly increase, affecting the effectiveness of network training. Finally, the number of available datasets for insulator defect detection is insufficient. Moreover, there are still some problems with low accuracy and low detection speed in insulator defect detection.

To solve the above problems, this paper proposes a defect detection method based on an improved YOLOv5s model for insulators with different sizes in the images under complex natural backgrounds. In this paper, the objects to be detected in the image are divided into two categories: insulator and defect. The insulator in categories refers to the entire insulator, regardless of whether it is damaged or not. The defect refers to the defect in the insulator. By directly detecting the insulators, the detection and localization of insulator defects can be achieved. Through performance comparison and analysis with traditional YOLOv5 models and other target detection algorithms, it demonstrates that the improved YOLOv5s model proposed in this paper can effectively identify and locate insulator defects of transmission lines under different environmental backgrounds.

The main contributions of this paper are summarized as follows:

- (1) This paper proposes an improved lightweight YOLOv5s method to detect and locate the insulator defects, which combines the GIoU loss function, Mish activation function, and CBAM attention mechanism modules to enhance detection accuracy.
- (2) The data enhancement method is utilized to enhance the generalization of the model, and the detection effect of the insulator defects with different sizes in the image are compared and verifies the proposed algorithm can effectively detect the insulator defect with different sizes, even small size defects.
- (3) This paper conducts the comparison analysis between the proposed method and conventional modules as well as different detection algorithms and demonstrates the proposed algorithm can not only accurately identify, but also locate the insulator defects under different environmental backgrounds.

The rest of the paper is organized as follows. Section 2 introduces the framework of the improved algorithm. Section 3 describes the experimental results. Section 4 discusses the results and conducts the comparison analysis. The conclusion and prospect of this paper are drawn in Section 5.

2. Insulator defect detection method based on improved YOLOv5s model

The whole process of the proposed insulator defect detection method is shown in Fig. 1. Firstly, the original insulator images are obtained through UAV aerial photography. Then, during the training process, the robustness of the proposed algorithm is enhanced through data enhancement. Then, input the insulator images into the proposed algorithm and obtain prediction results at three scales. Finally, the final results are screened through the non-maximum suppression (NMS) method.

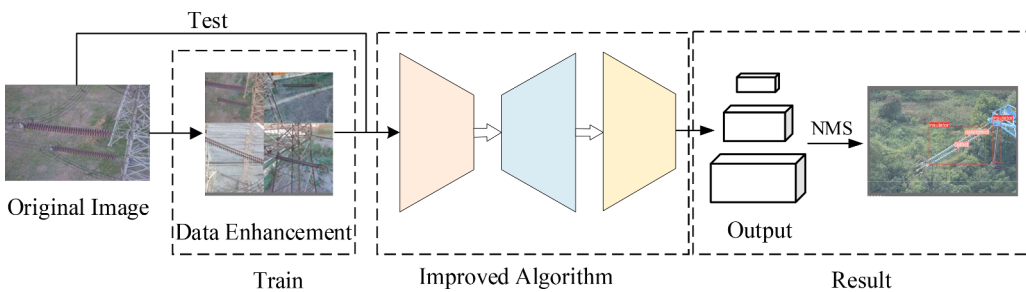


Fig. 1. The whole process of the proposed method.

2.1. Improved YOLOv5s model

The proposed improved YOLOv5 network is based on the YOLOv5s model. The network frame of the improved YOLOv5s model is shown in Fig. 2.

The proposed model extracts the features from the images through the CBS module and CSP module. The features form P1, P2, and P3 feature maps through down-sample in different levels. To fuse the detailed information and semantic information, P1 feature maps will be up-sample to match the size of P2 feature maps. This operation also occurs between P1 feature maps and P3 feature maps. Then detailed

information upward propagates to the semantic information to reduce information loss, and outputs can be obtained in three levels: output 1, output 2, and output 3. Output 1 mainly includes large-size targets, Output 2 includes medium-size targets, and Output 3 includes small-size targets.

2.2. Based network modules

YOLOv5s is the one whose feature map depth and width are the smallest in the YOLOv5 series [32]. The based YOLOv5s model mainly contains the following modules.

(1) CBS module

The CBS module is widely used in YOLOv5s's every position, as shown in Fig. 3. The CBS module is combined by Conv, BN, and SiLU, which conducts Conv, BN, and SiLU on input data in sequence.

(2) Resnet module

The Resnet module is mainly used in the CSP1 module, as shown in Fig. 4. It consists of two paths. One path passes through the CBS module twice, and another path does not have any operation. Finally, The Resnet module combines the data from the two paths at the dimension level.

(3) CSP1 module

The CSP1 module is mainly used in the backbone network, as shown in Fig. 5. The CSP1 module is formed by two paths. One path is composed of the CBS module and the Resnet module. The other uses a CBS module to adjust the channels and combine two paths. After the combining, output after a CBS module.

(4) CSP2 module

The CSP2 module is mainly used in the neck network, as shown in Fig. 6. The structure is similar to the CSP1 module, except the Resnet module is removed.

(5) SPPF module

The SPPF module is mainly used at the last step of the backbone network which integrates the features of different receptive fields by using parallel MAX pooling, as shown in Fig. 7. The SPPF module handles the input x by the CBS module and then gets y_1 after pooling, gets y_2 after pooling twice, and gets y_3 after pooling three times. Concat x , y_1 , y_2 , and y_3 in dimension, and output after the CBS module.

2.3. Improved modules

(1) GIoU loss function

Traditional YOLOv5s uses CIoU as the loss function. The improved YOLOv5 model utilizes the GIoU as the loss function. GIoU introduces a minimum closed rectangle that surrounds two bounding boxes based on IoU, which can calculate the loss value when the predicted box and the actual box do not intersect and has better detection performance for small targets, such as insulator defects.

The definition of GIoU can be expressed as,

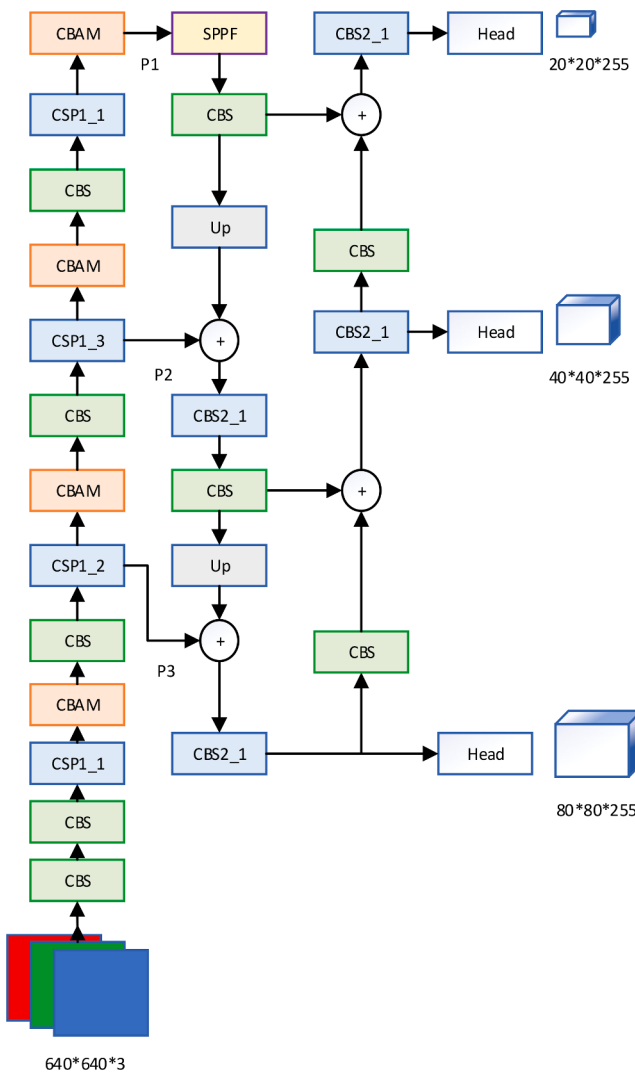


Fig. 2. Improved YOLOv5s model (CSP x _x is Cross Stage Partial module, CBAM is attention module, CBS is basic network module and Head is detect head).

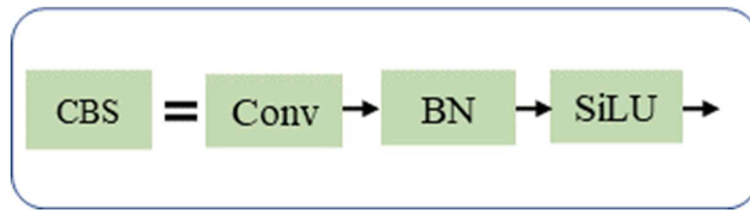


Fig. 3. CBS module.

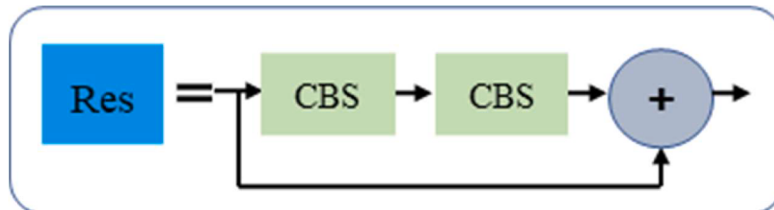


Fig. 4. Resnet module.

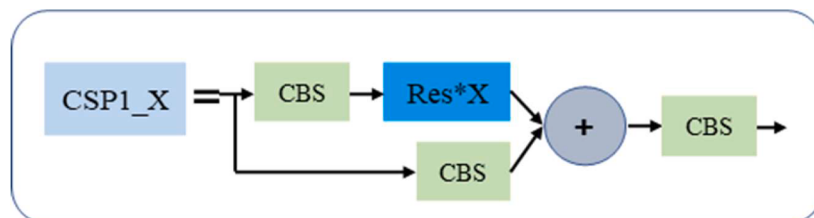


Fig. 5. CSP1 module.

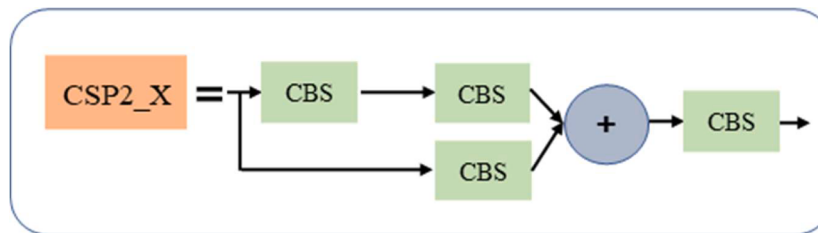


Fig. 6. CSP2 module.

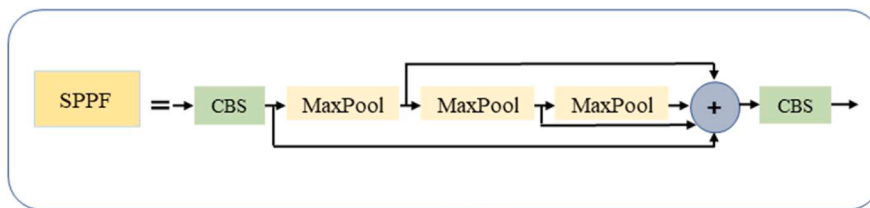


Fig. 7. SPPF module.

$$GIoU = IoU - \frac{|A_c - U|}{A_c} \quad (1)$$

Where IoU represents the intersection union ratio between the predicted box and the true box, A_c represents the area of the smallest closed rectangle between the predicted box and the true box, and U represents the area of the union between the predicted box and the true box.

(2) Mish activation function

The traditional TOLOv5s model uses SiLU as the activation function. The improved YOLOv5 model utilizes the Mish activation function to detect the insulator defects. The Mish activation function has no boundaries and can avoid saturation at gradients close to zero, and there is a certain negative value to prevent the death of the neural network nodes. Compared with SiLU, the Mish function not only has the same advantage as SiLU but also is smoother in the negative part, and converges faster than SiLU in the positive part, as shown in Figs. 8 and 9.

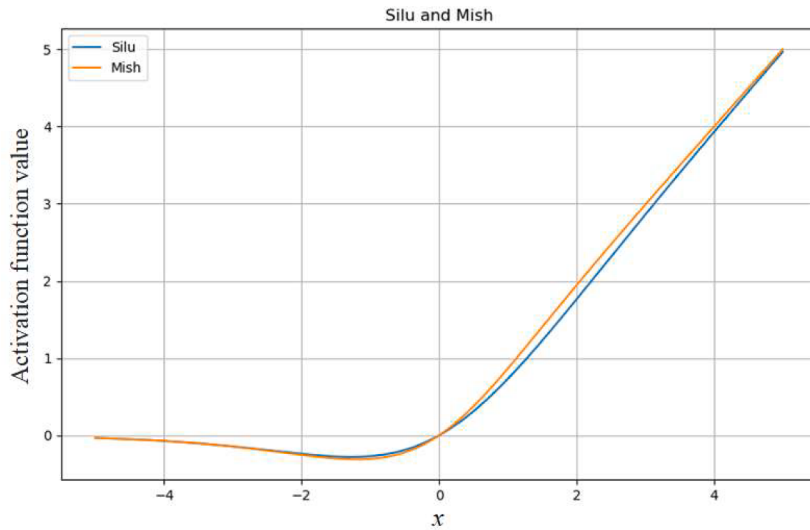


Fig. 8. SiLU and Mish.

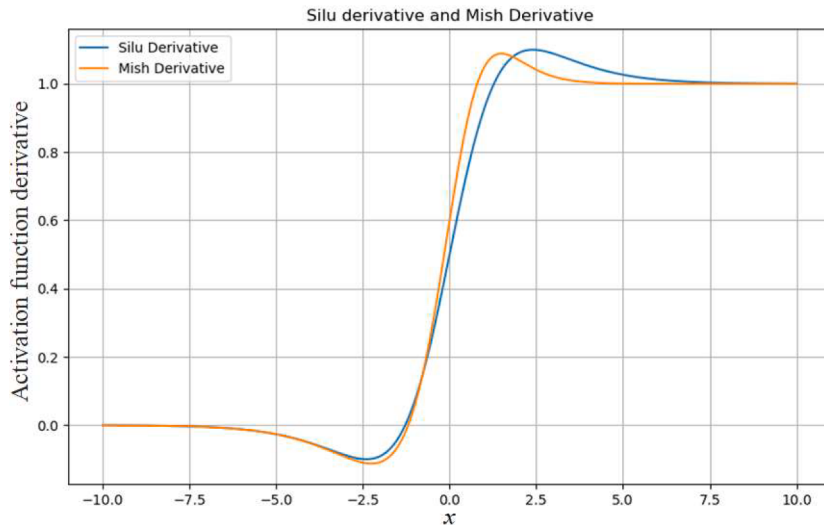


Fig. 9. SiLU derivative and Mish derivative.

$$SiLU(x) = \frac{x}{1 + e^{-x}} \quad (2)$$

$$Mish(x) = x * \tanh(\ln(1 + e^x)) \quad (3)$$

$$SiLU'(x) = \sigma(x) + x * \sigma(x)(1 - \sigma(x)) \quad (4)$$

$$Mish'(x) = \frac{e^x * (4(x+1) + 4e^{2x} + e^{3x} + e^x(4x+6))}{(2e^x + e^{2x} + 2)^2} \quad (5)$$

Where x is an input feature, $\sigma(x) = \frac{1}{1+e^{-x}}$

(3) Attention mechanism

The improved model utilizes the CBAM attention mechanism to enhance the accuracy of the insulator defect detection, as shown in Fig. 10. It inputs the result after the CSP1_X module to the channel attention mechanism module and spatial attention mechanism module, to self-adaptively study the features of the image containing the insulators and insulator defects from both spatial and channel perspectives. CBAM attention mechanism is mainly divided into two modules: channel attention mechanism and spatial attention mechanism [35]. Channel attention

mechanism firstly processes the input feature map through MAX pooling and Mean pooling, concatenates two results in dimension, then reduces the dimension through the convolution, and finally creates the feature map through the spatial attention mechanism module. The spatial attention mechanism makes the feature map through the channel attention module.

$$F' = M_C(F) \otimes F \quad (6)$$

$$F'' = M_S(F') \otimes F' \quad (7)$$

Where F is the feature map, M_C and M_S represent channel-based and spatial-based attention, \otimes represents element-wise multiplication, and F' , F'' represents the output feature map after channel attention and spatial attention, respectively.

2.4. Data enhancement

Since the accessible data of the insulators, especially the damaged

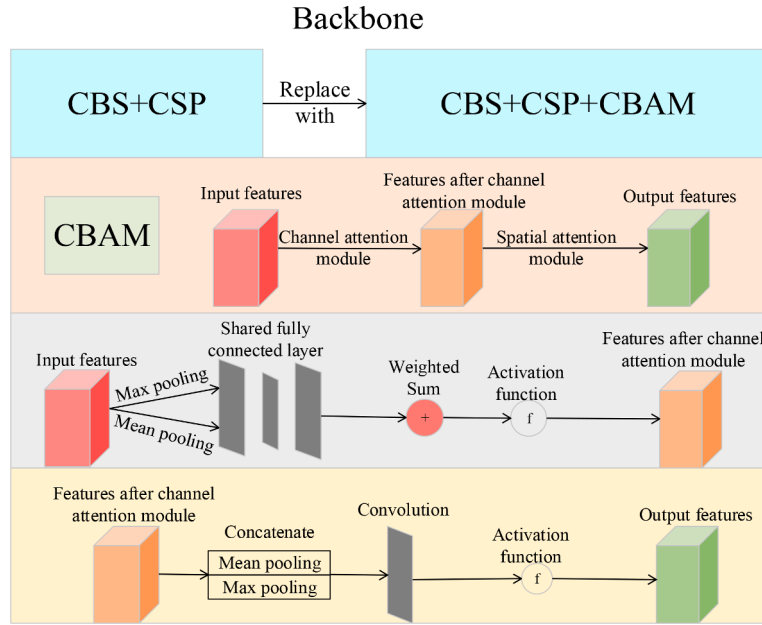


Fig. 10. CBAM attention mechanism.

insulators, is insufficient, it will weaken the detection effect of the proposed algorithm. To improve the generalization and robustness of the proposed algorithm, this paper utilizes data enhancement to produce more data, which consists of data enhancement at the pixel level and data enhancement at the image level.

Data enhancement at the pixel level contains HSV, scale, rotate, shear, etc. The insulator image enhanced by the four pixel-level methods is shown in Fig. 11. Data enhancement at the image level mainly is Mosaic. Mosaic is to randomly combine four random images into one image. The data enhancement at the image level is shown in Fig. 12.

2.5. Model performance indicators

To evaluate the detection accuracy of the proposed algorithm, the performance indicators including IoU, Precision, Recall, AP, and mAP are adopted.

The IoU is an indicator in evaluating the position accuracy in target

detection. It determines whether the target is found according to the degree of overlap between the candidate box and the real box. Its calculation formula is:

$$IoU = \frac{S_C \cap S_G}{S_C \cup S_G} \quad (8)$$

where S_G represents the real box, and S_C represents the predicted box.

After setting the IoU threshold, if the IoU of the prediction box and the real box is larger than the IoU threshold, the class of the prediction box fits the real class. If the confidence is larger than the confidence threshold, it will be regarded as the target is found correctly which is TP. If the IoU of the prediction box and the real box is smaller than the IoU threshold, the class of the prediction box doesn't fit the real class, it will be regarded as the target is found incorrectly which is FP. If there is a missing box, the number of missed targets is FN. Then the precision rate and recall rate can be calculated as,

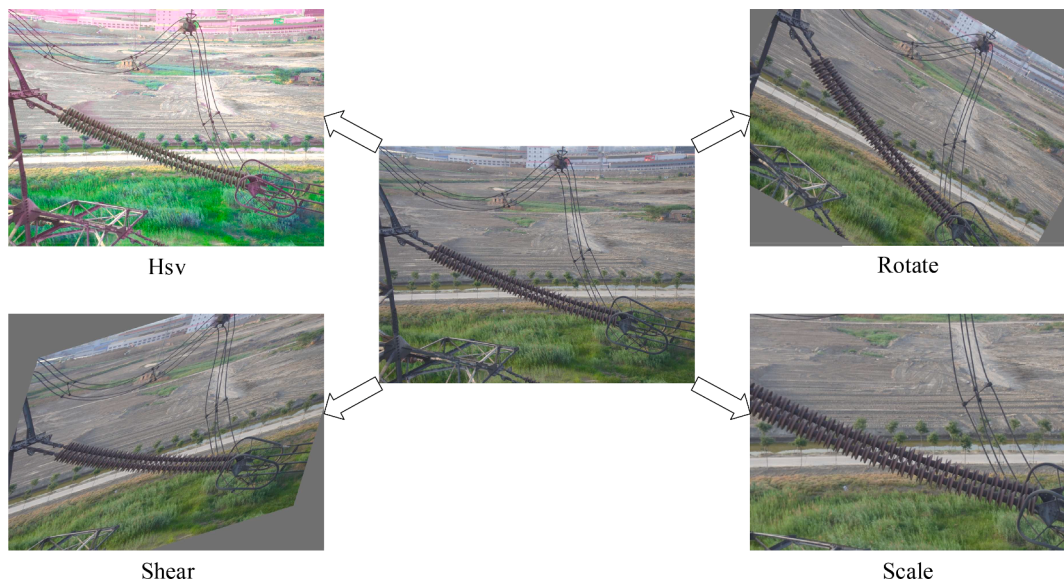


Fig. 11. Data enhancement at the pixel level.



Fig. 12. Data enhancement at the image level.

$$\begin{cases} Precision = \frac{TP}{TP + FP} \\ Recall = \frac{TP}{TP + FN} \end{cases} \quad (9)$$

where TP is true positive, FP is false positive, and FN is false negative.

Therefore, taking the accuracy rate as the vertical axis and the recall rate as the horizontal axis, the P-R curve can be obtained, and the area enclosed is the AP value of this category.

$$AP = \int_0^1 P(R)dR \quad (10)$$

mAP is the mean value of the AP value of each class. Since the classes of insulator defect detection in this paper are insulator and defect, the class number is 2.

$$mAP = \frac{1}{N} \sum AP \quad (11)$$

where N is the class number.

The detection speed is also an important performance indicator of the target detection algorithm. The common indicator is the frame per second (FPS), that is, the number of pictures that can be processed per second. The total detection time t can be obtained by testing n images in the test set, and then the FPS can be calculated:

$$FPS = \frac{n}{t} \quad (12)$$

where n is the number of the detected frames and t is the duration used for detection.

3. Experimental results

3.1. Insulator dataset

An insulator dataset used in this paper is provided by State Grid, which includes normal insulators and damaged insulators [36]. This dataset includes two kinds of insulators, as shown in Figs. 13 and 14. One kind of insulator is the normal insulator shot by UAV, whose number is 600. The other is a damaged insulator, whose number is 248.

For better training, some images are adjusted by the image process method, which transplants the damaged insulator to the background images. The concrete process is shown in Fig. 15. Firstly, cut the damaged insulator from the original image, and the result is the mask image. Then use affine transformation which performs a linear geometric transformation on the original coordinate to enhance the original image and mask to get the original mask image pair as the train data of U-Net [37]. Finally, train U-Net and use the trained U-Net to cut the image and connect the insulators from different environments. Finally, this paper has enhanced the dataset and expanded the dataset to 3409 images.

3.2. Train and testing for improved YOLOv5s model

3.2.1. Model train

To verify the proposed algorithm, this paper firstly tests the insulator defect detection algorithm based on the improved lightweight YOLOv5s model. First, the proposed algorithm is trained in the operator system of Ubuntu20 and the GPU environment of GeForce RTX 3060 12GB and uses pytorch1.10.2 as a support library of deep learning.

Then, to ensure the quality and efficiency of the train, this paper resizes the images to 640×640 , and allocates the dataset of 3409 images in the ratio of 8:1:1, according to the training set, verification set, and test set, respectively.

Then, extract the suitable anchors. Through the k-means method, the



Fig. 13. Normal insulators.



Fig. 14. Damaged insulators.

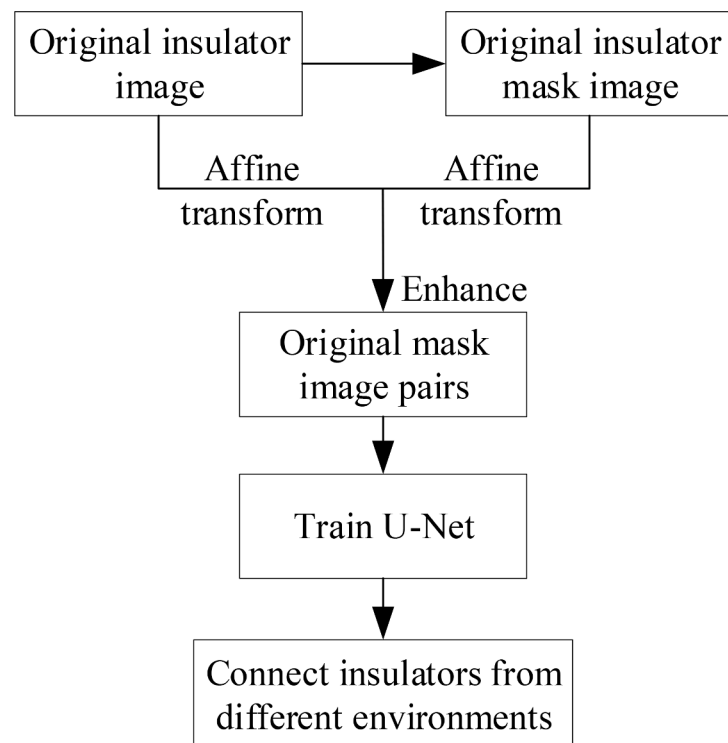


Fig. 15. Concrete process.

anchor that fits real train data better will be obtained. From the original dataset, randomly select k cluster centers to initialize, with k being 9 by default. Then distribute the boxes to the nearest cluster center, and update the cluster centers. Repeat the above until the cluster centers never change. After obtaining the anchor, calculate the Best Possible Recall (BPR). If the BPR ≥ 0.98 , that means the anchor gained is fit.

Before training, set the train parameters. In data enhancement, set three parameters of HSV color transformation are 0.015, 0.7, and 0.4, respectively. The scale of image scaling is 0.5, the flip probability is 0.5, and select mosaic to enhance the images. In the loss function part, the threshold of IoU in the training stage is 0.2. The return value of the loss function of the box is 0.05. The return value of the loss function of the class is 0.5. The return value of the loss function of obj is 0.5. In the learning rate part, the initialized learning rate is 0.01. The optimization operator is SGD and the momentum is 0.937, and the weight delay is 0.0005. In the train iteration part, the batch size of a single train is 16, and the number of epochs is 50.

Finally, input the dataset to the proposed algorithm to train. After 50 epochs of training, the error iteration curves of the training dataset and the testing dataset are shown in Fig. 16. The results show the proposed algorithm has been converged.

3.2.2. Model testing

Trains the proposed algorithm in 50 epochs. When the IoU threshold is 0.5:0.95 in 0.05 step size, the proposed algorithm performs well on the test dataset, and the AP value of the insulator reaches 80.3 %. The AP value of the defect reaches 38.5 % and the mAP value reaches 59.5 %. The proposed algorithm for detecting images reached 142 FPS. Hence, the proposed algorithm has achieved good results in terms of both detection accuracy and detection speed. When the detection speed keeps unchanging, the mAP value lifts to 60.1 %, the AP value of the insulator reaches 79.5 % and the AP value of the defect reaches 40.7 %.

4. Discussion and validation

4.1. Comparison with different modules

To verify the effectiveness of the proposed algorithm, this paper compares the performance between the proposed algorithm and traditional methods.

Firstly, this paper compares the performance with various loss functions, including GIoU, DIoU, EIoU [38], etc. The comparison results are shown in Table I. For insulator detection, since some insulators exhibit a high aspect ratio and the CIoU contains aspect loss, the CIoU can achieve the highest AP value in insulator detection. However, in defect detection, due to the small proportion of defects in the image, in the early training stage, there is a high probability of non-intersection between the predicted box and the real box, and the network cannot update the parameters. By adding a minimum bounding rectangle that introduces the predicted box and the real box, GIoU can update the network even when the predicted box and the real box do not intersect, resulting in better defect detection results. Since the aspect ratio of defect targets is relatively small, it cannot highlight the more prominent role of EIoU and CloU in aspect loss. Hence, the AP values of defect of DIoU, CloU, and EIoU are similar and all nearly 1.0 % lower than that of GIoU. Since the insulator defect detection is more important, even though the mAP 0.5:0.95 using GIoU is not the largest, the AP value in

Table I
Comparison results with different loss functions.

| Loss function | mAP 0.5:0.95(%) | AP: insulator (%) | AP: defect(%) |
|---------------|-----------------|-------------------|---------------|
| CIoU | 59.5 | 80.3 | 38.5 |
| DIoU | 58.8 | 78.9 | 38.6 |
| GIoU | 59.2 | 78.9 | 39.5 |
| EIoU | 58.7 | 78.8 | 38.6 |

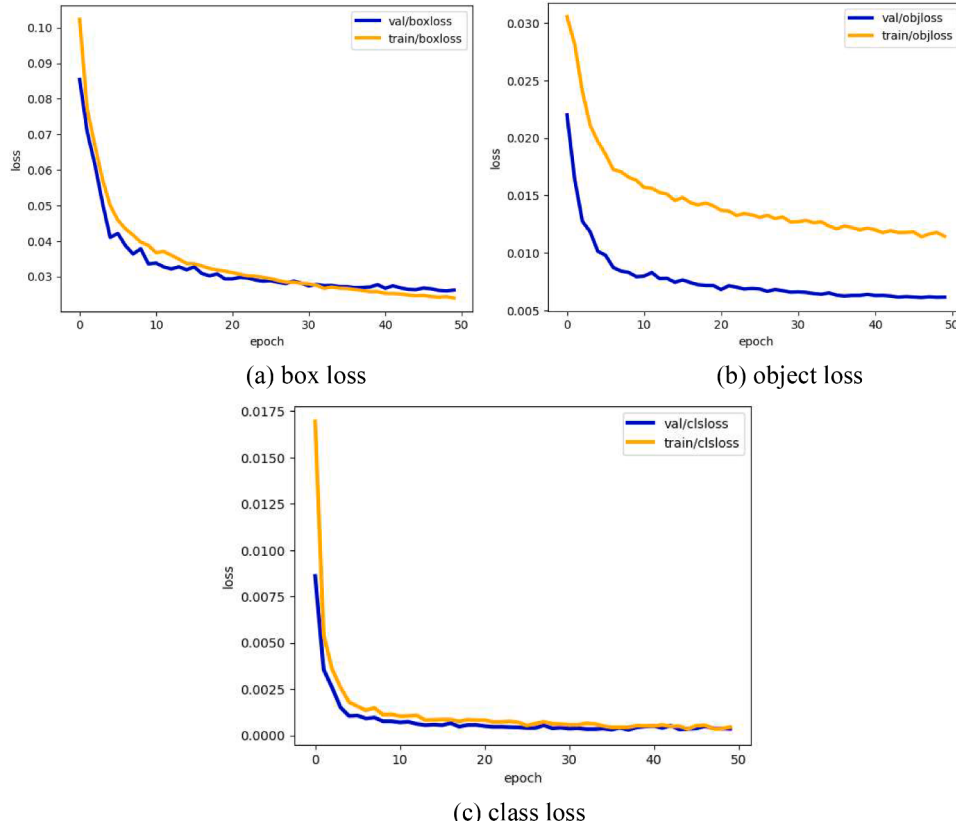


Fig. 16. Error iteration curves.

insulator defect detection is the largest, this paper selects the GIoU as the loss function. In addition, compared to DIoU and EIoU, the GIoU has the advantages of more concise representation, fewer training parameters, and easier training.

This paper also compares the performance with different activation functions, as shown in [Table II](#). Compared to ReLU, The Mish is continuously differentiable and can flow information more deeply due to its smoother gradient, resulting in better performance with a 40.7 % AP value of insulator defect detection. The HardSwish and FReLU have non-differentiable points, which may affect the transmission of gradient information and result in affecting some parts of the model that are not effectively updated during training. They have similar performance and cannot achieve good performance in insulator defect detection. Although Aconc smoothes the non-differentiable parts, it greatly increases computational complexity, which leads to poor performance of the algorithm in both insulator detection and defect detection. Hence, compared with other activation functions such as SiLU, HardSwish, FReLU, and Aconc, the Mish activation function has the highest mAP and AP: defect values, especially the AP: defect value can be improved by 2.2 %, while the AP value of insulator with SiLU is a little higher. Since it is more important for insulator defect detection, this paper chooses the Mish activation function for further testing.

To verify the performance of the attention mechanism, this paper compares the performance of whether the CBAM is introduced, as shown in [Table III](#). First, with the attention mechanism, the AP value of the defect reaches 43.4 % with a 2.7 % improvement, compared to that without the attention mechanism. It indicates that the introduction of CBAM effectively enhances the model's ability to identify insulator defects more accurately in complex environments. Secondly, the AP value of the insulator with the attention mechanism is similar to that without the attention mechanism. In UAV images, the insulator defects often exhibit small sizes, therefore it is crucial to improve the accuracy of small-object detection for insulator defect detection. The attention mechanism of CBAM enhances the key features and suppresses the irrelevant information, which helps the model better capture the details of small targets and improve detection accuracy. Hence, the results indicate that the CBAM has a significant improvement in insulator defect detection.

4.2. Comparison with different target detection algorithms

To validate the effectiveness of the proposed algorithm in this paper, a comparative analysis of the performance among various target detection algorithms has been conducted, as detailed in [Table IV](#). In terms of detection accuracy, compared with two-stage detection algorithms, such as the Faster RCNN algorithm, Sparse RCNN algorithm, and one-stage detection algorithm YOLOX without anchor frame, the improved algorithm proposed in this paper can achieve higher defect detection accuracy and higher FPS detection speed. Compared to Spark RCNN, traditional YOLOv5s has little difference in insulator detection accuracy and insulator defect detection accuracy. While YOLOv5s is a one-stage detection algorithm, which has a higher detection speed than that of Sparse RCNN while achieving close accuracy. YOLOX is an anchor-box-free algorithm that does not have pre-set anchor boxes for auxiliary detection, resulting in a stronger generalization of target sizes. However, the insulator defect sizes in the dataset are relatively uniform,

Table II
Comparison results with different activation functions.

| Activation function | mAP 0.5:0.95(%) | AP: insulator(%) | AP: defect(%) |
|---------------------|-----------------|------------------|---------------|
| SiLU | 59.5 | 80.3 | 38.5 |
| HardSwish | 58.1 | 78.9 | 38.0 |
| Mish | 60.1 | 79.5 | 40.7 |
| FReLU | 58.4 | 78.9 | 38.0 |
| Aconc | 56.4 | 75.6 | 37.2 |

Table III
Comparison results with the attention mechanism.

| | mAP 0.5:0.95 (%) | AP:Insulator (%) | AP: defect (%) |
|-----------------------------|------------------|------------------|----------------|
| Without attention mechanism | 60.1 | 79.5 | 40.7 |
| With attention mechanism | 61.3 | 79.2 | 43.4 |

Table IV
Comparison results with different target detection algorithms.

| Method | mAP 0.5:0.95 (%) | AP: Insulator (%) | AP :Defect (%) | FPS |
|-----------------|------------------|-------------------|----------------|-------|
| Faster RCNN | 31.7 | 51.3 | 12.2 | 6.1 |
| Sparse RCNN | 59.9 | 81.2 | 38.6 | 16.1 |
| YOLOX | 54.9 | 77.6 | 32.2 | 76.2 |
| YOLOv5s | 59.5 | 80.5 | 38.5 | 142.9 |
| Improved method | 61.3 | 79.2 | 43.4 | 142.9 |

and YOLOX's detection performance is worse than that of YOLOv5s. This paper improves the traditional YOLOv5s model to achieve better detection performance in insulator defect detection while maintaining a high detection speed. Compared with the traditional YOLOv5s model, the improved algorithm introduces the CBAM module to enhance the algorithm's attention to insulator defects and enhances the algorithm's learning ability on insulator defects by utilizing the Mish and GIoU functions. The AP value of default detection of the improved algorithm can be improved by 5 %.

[Fig. 17](#) shows the comparison of detection performance for an insulator. It shows, compared with other algorithms, the improved algorithm proposed in this paper has the best detection effect. Hence, the proposed algorithm for insulator defect detection has a good performance both in terms of insulator detection accuracy and detection speed, which can meet the actual requirements of transmission line UAV patrol inspection and has good application potential.

4.3. Validation with different insulator defect sizes

Based on the definition of small targets by the Society of Photo-Optical Instrumentation Engineers (SPIE), the target area of a small target in the 256×256 image is less than 80 pixels, in other words, the area ratio is less than 0.12 % [39]. Then, to verify the effectiveness of the proposed algorithm for different defect sizes, this paper divides the insulator defects into three categories based on their area proportion: small size (0, 0.12 %), medium size [0.12 %, 0.28 %], and large size (0.28 %, $+\infty$), and compares the detection effect with different defect sizes. [Fig. 18](#) shows the small-size defect, and the comparison results are shown in [Table V](#). Due to the distribution of the dataset, most of the defect sizes are concentrated in (0.0012, 0.0028), the proposed algorithm can perform better in defect detection with medium size. In defect detection with a small size, it can also achieve good performance with an AP value of 39.5 %.

4.4. Validation in different environmental backgrounds

To verify the robustness of the improved algorithm in different environment backgrounds, this paper processes the insulator images with different environmental backgrounds, which considers the rain and fog weather effects, adjusts the brightness of the image, and adds Gaussian noise to the images. The results are shown in [Table VI](#). From [Table VI](#), the fog, Gaussian noise, and rain seriously damage the integrity of insulators and have a greater impact on the detection accuracy. Hence, the insulator detection performance with the fog and Gaussian noise and rain are relatively worse, compared with that of the base, while the detection performances are acceptable for insulator defect

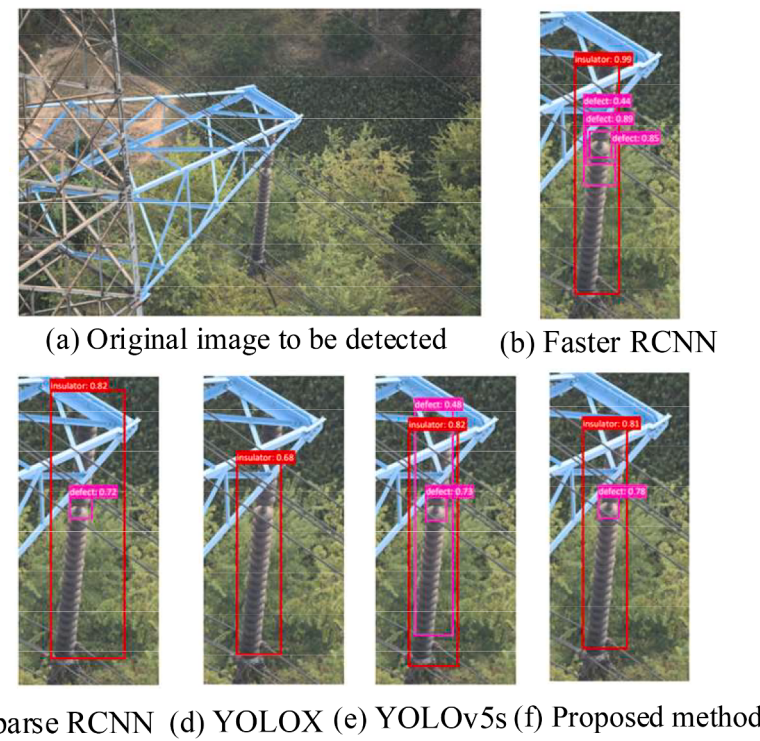


Fig. 17. Comparison of detection performance.



Fig. 18. Small-size defect.

Table V
Comparison results with different defect sizes.

| Defect size | mAP 0.5:0.95(%) | AP: insulator (%) | AP: defect(%) |
|-------------|-----------------|-------------------|---------------|
| Large size | 60.9 | 93.2 | 28.6 |
| Medium size | 66.2 | 86.4 | 45.9 |
| Small size | 56.1 | 72.5 | 39.5 |

detection. In addition, the dark and light effects just change the brightness of the insulator image, so they have little impact on the detection accuracy. Hence, although the rain, fog, and Gaussian noise have certain impacts on the detection performance, the improved algorithm can be well-adapted and robust to different environmental backgrounds.

Table VI
Comparison results with different environmental backgrounds.

| Background | mAP 0.5:0.95(%) | AP: Insulator(%) | AP :Defect(%) |
|----------------|-----------------|------------------|---------------|
| Base | 61.3 | 79.2 | 43.4 |
| Rain | 57.7 | 76.5 | 38.9 |
| Fog | 56.8 | 75.8 | 37.8 |
| Dark | 60.8 | 79.2 | 42.3 |
| Light | 60.7 | 78 | 43.4 |
| Gaussian noise | 56.6 | 75.7 | 37.5 |

5. Conclusion

This paper proposes an improved lightweight YOLOv5s model for insulator defect detection in complex backgrounds captured by UAV aerial photography, which has the advantages of high detection accuracy and fast detection speed. The improved algorithm utilizes a CBAM

module to enhance the algorithm's attention to insulator defects and enhances the algorithm's learning ability on insulator defects by using Mish and GIoU. Compared with other conventional modules, the AP value of defect with the GIoU, Mish function, and CBAM module can be improved by 1.0 %, 2.2 %, and 2.7 %, respectively. Besides, this paper compares the performance with different target detection algorithms and tests the improved algorithm in different environmental backgrounds. Compared with traditional methods, the accuracy of the proposed algorithm in detecting insulator defects can be effectively improved, and the AP value of default detection of the improved method can be increased by 5 %. Moreover, although the rain, fog, and Gaussian noise have certain impacts on the detection performance, the improved algorithm can be well-adapted and robust to different environmental backgrounds. Hence, the results demonstrate that the improved algorithm proposed in this paper can effectively identify and locate insulator defects under different environmental backgrounds.

In addition, it's worth noting that there are still some limitations on the types of insulator detection and detection accuracy for this research. In the future, this paper will study insulator defect detection with different types of defects, improve the detection accuracy and efficiency of the proposed algorithm with other modules, and consider the factors of computational power, model size, and complexity. Moreover, the hyperparameter optimization algorithms would be adopted to optimize the parameters for better parameter selection in future research.

CRediT authorship contribution statement

Liangliang Wei: Writing – review & editing, Writing – original draft, Validation, Investigation, Funding acquisition, Conceptualization. **Jun Jin:** Writing – original draft, Methodology, Investigation. **Kaiyuan Deng:** Writing – original draft, Methodology, Investigation, Formal analysis, Data curation. **Han Liu:** Writing – review & editing, Writing – original draft, Validation, Software, Methodology, Investigation, Conceptualization.

Declaration of competing interest

The authors declare that they have no known competing financial interests or personal relationships that could have appeared to influence the work reported in this paper.

Data availability

Data will be made available on request.

References

- [1] M.-R. Halloum, B. Subba Reddy, Failure analysis of polymeric outdoor insulators used in HVDC converter stations, *Eng. Fail. Anal.* 158 (2024) 108051, <https://doi.org/10.1016/j.engfailanal.2024.108051>. Apr.
- [2] G. Fotis, V. Vita, G. Milushev, et al., After installation testing and fault detection during the operation of HV submarine power cables, in: 2023 15th Electrical Engineering Faculty Conference (BulEF), Varna, Bulgaria, 2023, pp. 1–5, <https://doi.org/10.1109/BulEF59783.2023.10406267>. Sep.
- [3] S. Deb, S. Lata, V.S. Bhadoria, et al., Improved relay algorithm for detection and classification of transmission line faults in monopolar HVDC transmission system using signum function of transient energy, *IEEE Access* 12 (2024) 15561–15571, <https://doi.org/10.1109/ACCESS.2024.3356012>. Jan.
- [4] H. Guan, X. Sun, Y. Su, et al., UAV-lidar aids automatic intelligent powerline inspection, *Int. J. Electr. Power Energy Syst.* 130 (2021) 106987, <https://doi.org/10.1016/j.ijepes.2021.106987>. Sep.
- [5] B. Dolník, L. Sárpataky, S. Bucko, M. Pavlík, R. Štefko, Assessing contamination severity of high voltage insulators using dielectric loss factor: laboratory measurements and comparative analysis of leakage current and dielectric loss factor at different voltage levels, humidity, and insulating materials, *Electr. Power Syst. Res.* 225 (2023) 109855, <https://doi.org/10.1016/j.epsr.2023.109855>.
- [6] A.B. Alhassan, X. Zhang, H. Shen, et al., Power transmission line inspection robots: a review, trends and challenges for future research, *Int. J. Electr. Power Energy Syst.* 118 (2020) 105862, <https://doi.org/10.1016/j.ijepes.2020.105862>. Jun.
- [7] MD.F. Ahmed, J.C. Mohanta, A. Sanyal, Inspection and identification of transmission line insulator breakdown based on deep learning using aerial images, *Electr. Power Syst. Res.* 211 (2022) 108199, <https://doi.org/10.1016/j.epsr.2022.108199>. Oct.
- [8] Z. Li, L. Ding, J. Liu, UV detection technology of insulator discharge based on UAV platform, in: 2022 IEEE International Conference on Electrical Engineering, Big Data and Algorithms (EEBDA), Changchun, China, 2022, pp. 261–265, <https://doi.org/10.1109/EEBDA53927.2022.9744897>.
- [9] C. Wang, H. Pei, G. Tang, et al., Pointer meter recognition in UAV inspection of overhead transmission lines, *Energy Rep.* 8 (2022) 243–250, <https://doi.org/10.1016/j.egyr.2022.02.108>. Aug.
- [10] K. Li, X. Yan, Y. Han, Multi-mechanism swarm optimization for multi-UAV task assignment and path planning in transmission line inspection under multi-wind field, *Appl. Soft Comput.* 150 (2024) 111033, <https://doi.org/10.1016/j.asoc.2023.111033>. Jan.
- [11] L. Yin, J. Hu, W.B. Wang, et al., Parameters Optimization of UAV for Insulator Inspection on Power Transmission Line, *IEEE Access* 10 (2022) 97022–97029, <https://doi.org/10.1109/ACCESS.2022.3192643>. Jul.
- [12] J. Liu, M. Hu, J. Dong, X. Lu, Summary of insulator defect detection based on deep learning, *Electr. Power Syst. Res.* 224 (2023) 109688, <https://doi.org/10.1016/j.epsr.2023.109688>.
- [13] S. Liao, J. An, A robust insulator detection algorithm based on local features and spatial orders for aerial images, *IEEE Geosci. Remote Sens. Lett.* 12 (5) (2015) 963–967, <https://doi.org/10.1109/LGRS.2014.2369525>. May.
- [14] Y. Yu, H. Cao, Z. Wang, et al., Texture-and-shape based active contour model for insulator segmentation, *IEEE Access* 7 (2019) 78706–78714, <https://doi.org/10.1109/ACCESS.2019.2922257>. Jun.
- [15] Q. Wu, J. An, An active contour model based on texture distribution for extracting inhomogeneous insulators from aerial images, *IEEE Geosci. Remote Sens.* 52 (6) (2014) 3613–3626, <https://doi.org/10.1109/TGRS.2013.2274101>. Jun.
- [16] M.T. Gencoglu, M. Uyar, Prediction of flashover voltage of insulators using least squares support vector machines, *Expert Syst. Appl.* 36 (7) (2009) 10789–10798, <https://doi.org/10.1016/j.eswa.2009.02.021>. Sep.
- [17] V.S. Murthy, K. Tarakanath, D.K. Mohanta, et al., Insulator condition analysis for overhead distribution lines using combined wavelet support vector machine (svm), *IEEE Trans. Dielectr. Electr. Insul.* 17 (1) (2010) 89–99, <https://doi.org/10.1109/TDEI.2010.5412006>. Feb.
- [18] L. Singh, A. Alam, K.V. Kumar, D. Kumar, P. Kumar, Z.A. Jaffery, Design of thermal imaging-based health condition monitoring and early fault detection technique for porcelain insulators using machine learning, *Environ. Technol. Innov.* 24 (2021) 102000, <https://doi.org/10.1016/j.eti.2021.102000>. Nov.
- [19] Z. Yang, Z. Xu, Y. Wang, Bidirection-fusion-yolov3: an improved method for insulator defect detection using uav image, *IEEE Trans. Instrum. Meas.* 71 (2022) 3521408, <https://doi.org/10.1109/TIM.2022.3201499> art. noAug.
- [20] S. Ren, K. He, R. Girshick, J. Sun, Faster R-CNN: towards real-time object detection with region proposal networks, *IEEE Trans. Pattern Anal. Mach. Intell.* 39 (6) (2017) 1137–1149, <https://doi.org/10.1109/TPAMI.2016.2577031>. Jun.
- [21] X. Lei, Z. Sui, Intelligent fault detection of high voltage line based on the Faster RCNN, *Measurement* 138 (2019) 379–385, <https://doi.org/10.1016/j.measurement.2019.01.072>. May.
- [22] K. Hao, G. Chen, L. Zhao, et al., An insulator defect detection model in aerial images based on multiscale feature pyramid network, *IEEE Trans. Instrum. Meas.* 71 (2022) 3522412, <https://doi.org/10.1109/TIM.2022.3200861> art. noAug.
- [23] S. Dian, X. Zhong, Y. Zhong, Faster R-Transformer: an efficient method for insulator detection in complex aerial environments, *Measurement* 199 (2022) 111238, <https://doi.org/10.1016/j.measurement.2022.111238> art. noAug.
- [24] Z. Chen, H. Guo, J. Yang, et al., Fast vehicle detection algorithm in traffic scene based on improved SSD, *Measurement* 201 (2022) 111655, <https://doi.org/10.1016/j.measurement.2022.111655> art. no.
- [25] J. Redmon, S. Divvala, R. Girshick, A. Farhadi, You only look once: unified, real-time object detection, in: 2016 IEEE Conference on Computer Vision and Pattern Recognition (CVPR), 2016, pp. 779–788, <https://doi.org/10.1109/CVPR.2016.91>.
- [26] Y. Zhang, Y. Yang, J. Sun, R. Ji, P. Zhang, H. Shan, Surface defect detection of wind turbine based on lightweight YOLOv5s model, *Measurement* 220 (2023) 113222, <https://doi.org/10.1016/j.measurement.2023.113222> art. noJun.
- [27] J. Jiang, Z. Yang, C. Wu, Y. Guo, M. Yang, W. Feng, A compatible detector based on improved YOLOv5 for hydropower device detection in AR inspection system, *Expert Syst. Appl.* 225 (2023) 120065, <https://doi.org/10.1016/j.eswa.2023.120065>.
- [28] X. Miao, X. Liu, J. Chen, et al., Insulator detection in aerial images for transmission line inspection using single shot multibox detector, *IEEE Access* 7 (2019) 9945–9956, <https://doi.org/10.1109/ACCESS.2019.2891123>. Jan.
- [29] H. Chen, Z. He, B. Shi, T. Zhong, Research on recognition method of electrical components based on YOLO V3, *IEEE Access* 7 (2019) 157818–157829, <https://doi.org/10.1109/ACCESS.2019.2950053>.
- [30] H. He, et al., An insulator self-blast detection method based on YOLOv4 with aerial images, *Energy Rep.* 8 (2022) 448–454, <https://doi.org/10.1016/j.egyr.2021.11.115>. Apr.
- [31] G. Han, M. He, M. Gao, et al., Insulator breakage detection based on improved yolov5, *Sustainability* 14 (20) (2022) 5176, <https://doi.org/10.3390/su14106066>, art. May.
- [32] M. Zhou, B. Li, J. Wang, S. He, Fault detection method of glass insulator aerial image based on the improved YOLOv5, *IEEE Trans. Instrum. Meas.* 72 (2023) 1–10, <https://doi.org/10.1109/TIM.2023.3269099>.
- [33] Z. Huang, S. Hu, L. Zhang, Fault detection of insulator in distribution network based on YOLOv5s neural network, in: 2022 International Conference on Artificial

- Intelligence and Computer Information Technology (AICIT), 2022, pp. 1–5, <https://doi.org/10.1109/AICIT5386.2022.9930315>. Sep.
- [34] L. Yang, J. Fan, S. Song, et al., A light defect detection algorithm of power insulators from aerial images for power inspection, *Neural Comput. Appl.* 34 (20) (2022) 17951–17961, <https://doi.org/10.1007/s00521-022-07437-5>. Jun.
- [35] J. Qu, Q. Sun, Z. Qian, L. Wei, H. Zareipour, Fault diagnosis for PV arrays considering dust impact based on transformed graphical features of characteristic curves and convolutional neural network with CBAM modules, *Appl. Energy* 355 (2024) 122252, <https://doi.org/10.1016/j.apenergy.2023.122252>. Feb.
- [36] X. Tao, D. Zhang, Z. Wang, X. Liu, H. Zhang, D. Xu, Detection of power line insulator defects using aerial images analyzed with convolutional neural networks, *IEEE Trans. Syst. Man Cybern. Syst.* 50 (4) (2020) 1486–1498, <https://doi.org/10.1109/TSMC.2018.2871750>. Apr.[30].
- [37] O. Ronneberger, P. Fischer, T. Brox, U-Net: convolutional networks for biomedical image segmentation,” in *medical image computing and computer-assisted intervention – MICCAI 2015*, in: N. Navab, J. Hornegger, W.M. Wells, A.F. Frangi (Eds.), Lecture Notes in Computer Science, Springer International Publishing, Cham, 2015, pp. 234–241, https://doi.org/10.1007/978-3-319-24574-4_28.
- [38] Y. Zhang, W. Ren, Z. Zhang, Z. Jia, L. Wang, T. Tan, Focal and efficient IOU loss for accurate bounding box regression, *Neurocomputing* 506 (2022) 146–157, <https://doi.org/10.1016/j.neucom.2022.07.042>. Sep.
- [39] C. Li, Z. Huang, X. Xie, et al., IST-TransNet: infrared small target detection based on transformer network, *Infrared Phys. Techn.* 132 (2023) 104723, <https://doi.org/10.1016/j.infrared.2023.104723> art. noAug.